# Supporting Information

# A Metal–Organic Framework Based Propylene Nano-trap with Dual Functionalities for Highly Efficient Propylene/Propane Separation

Hui-Min Wen[a], Miaoyu Liu[a], Yujia Ling[a], Xiao-Wen Gu[b], Di Liu[b], Chenyi Yu[a], Yulan Liang[a], Bo Xie[a], Bin Li*[b], and Jun Hu*[a]

[a] College of Chemical Engineering, Zhejiang University of Technology, Hangzhou 310014, China. Email: hjzjut@zjut.edu.cn

[b] State Key Laboratory of Silicon and Advanced Semiconductor Materials, School of Materials Science and Engineering, Zhejiang University, Hangzhou 310027, China. E-mail: bin.li@zju.edu.cn

# Table of Contents

# Supplementary Experimental section

## 1. General procedures and materials

All starting reagents and solvents were purchased from commercial companies and used without further purification. Nickel hexafluorosilicate ($NiSiF_6$, CAS: 26043-11-8) was purchased from Energy Chemical, and 2-mercaptopyrazine (pyz-SH, CAS: 38521-06-1) was purchased from Macklin. Powder X–ray diffraction (PXRD) patterns were measured by a Rigaku Ultima IV diffractometer operated at 40 kV and 44 mA with a scan rate of 2 deg $min^{-1}$. Thermogravimetric analysis (TGA) was performed on a Netzsch TG209F3 instrument and the sample was heated under $N_2$ atmosphere with a heating rate of 5 K $min^{-1}$.

$CO_2$ (99.995%), $C_3H_6$ (99.5%), $C_3H_8$ (99.9%), He (99.999%) and mixed gases of $C_3H_6/C_3H_8$ = 50/50 (v/v) and $C_3H_6/C_3H_8$ = 10/90 (v/v) were purchased from JinGong Company (China).

## 2. Synthesis of $[Ni(pyz\text{-}SH)_2(SiF_6)]_n$ (ZJUT-2)

The powder samples of ZJUT-2 were synthesized using the same methods reported in the corresponding literature.[1] $[Ni(pyz\text{-}SH)_2(SiF_6)]_n$ (ZJUT-2) was synthesized by the solvothermal reaction of nickel hexafluorosilicate ($NiSiF_6$, 0.67 mmol) with 2-mercaptopyrazine (pyz-SH, 0.67 mmol) in 20 mL methanol at 85 ℃. Light-yellow powder was obtained after 48 h, collected by filtration and then washed with methanol. Bulk purity of the sample was verified by PXRD.

## 3. Gas sorption measurements

Gas adsorption isotherms were measured by Micromeritics ASAP 2020 surface area analyzer. To remove all the guest solvents in the framework, the fresh powder sample was first solvent-exchanged with dry methanol at least 8 times within three days. The solvent-exchanged sample was evacuated at room temperature (298 K) for 24 h, and then at 323 K for additional 12 h until the outgas rate was 5 μmHg $min^{-1}$ prior to measurements. The sorption measurement was maintained at 77 K with liquid nitrogen.

An ice-water bath (slush) and water bath were used for adsorption isotherms at 273 and 296 K, respectively.

## 4. Fitting of pure component isotherms

The pure component isotherm data for $C_3H_6$ and $C_3H_8$ in ZJUT-2a at 296 K were fitted with the single-site Langmuir-Freundlich isotherm model

$$q = q_{sat}\frac{bp^{\nu}}{1+bp^{\nu}} \tag{1}$$

with $T$-dependent parameter $b$

$$b = b_0 \exp\left(\frac{E}{RT}\right) \tag{2}$$

The fitted parameters are provided in Table S1.

## 5. Virial Graph Analysis

Estimation of the isosteric heats of gas adsorption ($Q_{st}$)

A virial-type expression of comprising the temperature-independent parameters $a_i$ and $b_j$ was employed to calculate the enthalpies of adsorption for $C_3H_6$ and $C_3H_8$ (at 273 K, 296 K) on ZJUT-2a. In each case, the data were fitted with equation:

$$\ln P = \ln N + 1/T\sum_{i=0}^{m} a_i N_i + \sum_{j=0}^{n} b_j N_j \tag{3}$$

Here, $P$ is the pressure expressed in mmHg, $N$ is the amount absorbed in mmol $g^{-1}$, $T$ is the temperature in K, $a_i$ and $b_j$ are virial coefficients, and $m$, $n$ represent the number of coefficients required to adequately describe the isotherms ($m$ and $n$ were gradually increased till the contribution of extra added $a$ and $b$ coefficients were deemed to be statistically insignificant towards the overall fit. And the average value of the squared deviations from the experimental values was minimized). The values of the virial coefficients $a_0$ to $a_m$ were then used to calculate the isosteric heat of absorption using the following expression:

$$Q_{st} = -R\sum_{i=0}^{m} a_i N_i \quad (4)$$

$Q_{st}$ is the coverage-dependent isosteric heat of adsorption and $R$ is the universal gas constant. The heat enthalpies of $C_3H_6$ and $C_3H_8$ sorption for complex ZJUT-2a in this manuscript are determined by using the sorption data measured in the pressure range from 0-1 bar (at 273 K, 296 K).

## 6. IAST calculations

The adsorption selectivity was predicted by using the Ideal Adsorbed Solution Theory (IAST) of Myers and Prausnitz.[2] The adsorption selectivity is defined by

$$S_{ads} = \frac{q_1/q_2}{p_1/p_2} \quad (5)$$

In equation (5), $q_1$ and $q_2$ are the molar loadings of the adsorbed phase in equilibrium with the bulk gas phase with partial pressures $p_1$ and $p_2$. The IAST calculation results of the adsorption selectivity of 50/50 (v/v) $C_3H_6/C_3H_8$ and 10/90 (v/v) $C_3H_6/C_3H_8$ for ZJUT-2a at 296 K are shown in Figure 2e.

## 7. Computational results and details

In order to obtain the reasonable binding sites of gas molecules in ZJUT-2a for subsequent modeling, Grand Canonical Monte Carlo (GCMC) simulations were performed in the MS modeling. The crystal structures of ZJUT-2a were chosen for related simulations without further geometry optimization. The framework and the individual $C_3H_6$ and $C_3H_8$ molecules were considered to be rigid during the simulation. Partial charges for atoms of guest-free ZJUT-2a were derived from QEq method and QEq_neutral1.0 parameter. The simulations were carried out at 296 K, adopting the locate task, Metropolis method in Sorption module and the universal force field (UFF). The partial charges on the atoms of $C_3H_6$ (C1: −0.276e, C2: −0.141e, C6: −0.401; H3: 0.146e, H4: 0.124e, H5: 0.142e, H7: 0.124e, H8: 0.141e, H9: 0.141e, where e = $1.6022 \times 10^{-19}$ C is the elementary charge) and $C_3H_8$ (C1: −0.430e, C2: −0.295e, C7: −0.430;

H3: 0.147e, H4: 0.147e, H5: 0.128e, H6: 0.157e, H8: 0.157e, H9: 0.128e, H10: 0.147e, H11: 0.147e) were also derived from QEq method. The interaction energy between hydrocarbon molecules and framework were computed through the Coulomb and Lennard-Jones 6-12 (LJ) potentials. The cutoff radius was chosen as 12.5 Å for the LJ potential and the long-range electrostatic interactions were handled using the Ewald & Group summation method. The loading steps and the equilibration steps were $1 \times 10^5$, the production steps were $1 \times 10^6$.

## 8. Breakthrough experiments

The breakthrough experiments were performed in dynamic gas breakthrough equipment using two stainless steel columns (4.0 mm inner diameter × 150 mm for 50/50 $C_3H_6/C_3H_8$ mixture and 4.0 mm inner diameter × 120 mm for 10/90 $C_3H_6/C_3H_8$ mixture). The weights of sample packed in the columns were 1.2535 g and 0.6258 g, respectively. The columns were activated under reduced pressure at 323 K overnight. The experimental set-up consisted of two fixed-bed stainless steel reactors. One reactor was loaded with the adsorbent, while the other reactor was used as a blank control group to stabilize the gas flow. The gas flows were controlled at the inlet by a mass flow meter as 2 mL $min^{-1}$, and a gas chromatograph (TCD-Thermal Conductivity Detector, detection limit 0.1 ppm) continuously monitored the effluent gas from the adsorption bed. Prior to every breakthrough experiment, we activated the sample by flushing the adsorption bed with helium gas for 2 hours at 373 K. Subsequently, the column was allowed to equilibrate at the measurement rate before we switched the gas flow.

## 9. Gas equilibrium adsorption capacity and separation factor

The complete breakthrough of $C_3H_6$ was indicated by the downstream gas composition reaching that of the feed gas. On the basis of the mass balance, the gas adsorption capacities can be determined as follows:

$$q_i = \frac{C_i V}{22.4 \times m} \times \int_0^t \left(1 - \frac{F}{F_0}\right) dt \tag{6}$$

Where $q_i$ is the equilibrium adsorption capacity of gas $i$ (mmol $g^{-1}$), $C_i$ is the feed gas concentration, $V$ is the volumetric feed flow rate ($cm^3$ $min^{-1}$), $t$ is the adsorption time (min), $F_0$ and $F$ are the inlet and outlet gas molar flow rates, respectively, and $m$ is the mass of the adsorbent (g). The separation factor (α) of the breakthrough experiment is determined as:

$$\alpha = \frac{q_A y_B}{q_B y_A} \tag{7}$$

in which $y_i$ is the molar fraction of gas $i$ ($i$ = A, B) in the gas mixture.

## Notation

| | |
|---|---|
| $q_i$ | component molar loading of species *i*, mol kg$^{-1}$ |
| $q_{sat}$ | saturation loading, mol kg$^{-1}$ |
| $b$ | Langmuir-Freundlich constant, kPa$^{-v}$ |
| $p_i$ | partial pressure of species *i* in mixture, kPa |
| $p_t$ | total system pressure, kPa |
| $T$ | absolute temperature, K |

## Greek letters

| | |
|---|---|
| $v$ | Freundlich exponent, dimensionless |

# Supplementary Tables

**Table S1.** Single-site Langmuir-Freundlich parameter fits for $C_3H_6$ and $C_3H_8$ in ZJUT-2a. The fits are based on experimental isotherm data at 296 K.

| | $q_{sat}$ | $b_0$ | $\nu$ |
|---|---|---|---|
| | mol kg$^{-1}$ | $_k$Pa$^{-\nu A}$ | dimensionless |
| $C_3H_6$ | 4.55284 | 0.25785 | 0.49151 |
| $C_3H_8$ | 3.08133 | 0.00164 | 1.73149 |

**Table S2.** Comparison of the $C_3H_6$ uptake, IAST selectivity and $Q_{st}$ of $C_3H_6$ for ZJUT-2a and some top-performing MOFs reported for $C_3H_6/C_3H_8$ separation.

| MOFs | $T$ (K) | $C_3H_6$ Uptake[a] ($cm^3\ cm^{-3}$) | | | 50/50 $C_3H_6/C_3H_8$ IAST selectivity[b] | $Q_{st}$ of $C_3H_6$[c] ($kJ\ mol^{-1}$) | Ref. |
|---|---|---|---|---|---|---|---|
| | | 1 bar | 0.5 bar | 0.1 bar | | | |
| **ZJUT-2a** | **296** | **138.9** | **123.5** | **72.3** | **17.2** | **45** | **This work** |
| $Co_2$(*m*-dobdc) | 298 | 201.9 | 196.6 | 183.0 | 38 | 56 | 3 |
| Co-MOF-74 | 298 | 191.4 | 185.9 | 136.9 | 45 | --[d] | 4 |
| GeFSIX-2-Cu-i | 298 | 88.4 | 76.2 | 37.8 | 4 | 32.1 | 5 |
| SIFSIX-2-Cu-i | 298 | 74.6 | 61.9 | 28.2 | 4.5 | 35.8 | 5 |
| Co-gallate | 298 | 66.6 | 50.1 | 12 | 333 | 41.0 | 6 |
| HIAM-301 | 298 | 93.0 | 87.2 | 71.5 | 150 | 27 | 7 |
| Y-abtc | 298 | 63.5 | 62.7 | 53.7 | --[d] | 50.0 | 8 |
| $Co(AIP)(BPY)_{0.5}$ | 298 | 63.8 | 58.0 | 26.2 | 21 | 42.4 | 9 |
| KAUST-7 | 298 | 56.8 | 46.0 | 9.41 | --[d] | 57.4 | 10 |
| MAF-23-O | 298 | 45.1 | 44.1 | 36.3 | 8.8 | 54 | 11 |
| UTSA-400 | 298 | 92.1 | 85.5 | 46.3 | $10^7$ | 60.5 | 12 |
| JNU-3a | 303 | 79.2 | 69.3 | 17.3 | 513 | 29.3 | 13 |
| MFM-520 | 298 | 78 | 74.6 | 67.4 | 17 | 48.5 | 14 |
| ZJU-75a | 296 | 104.3 | 90.5 | 71.2 | 54.2 | 65.9 | 15 |

[a] Adsorption capacity is obtained from single-component gas adsorption isotherms.

[b] Selectivity is calculated by the IAST method for an equimolar mixture at 1 bar.

[c] $Q_{st}$ values at near-zero coverage.

[d] The value was not reported in the literature, which shows molecular sieving effect.

**Table S3.** Comparison of the $C_3H_6$ dynamic uptake and selectivity based on 50/50 $C_3H_6/C_3H_8$ breakthrough curves for ZJUT-2a and other reported materials.

| MOFs | $C_3H_6$ dynamic uptake (mmol $g^{-1}$)[a] | $C_3H_6/C_3H_8$ dynamic selectivity[b] | Ref. |
|---|---|---|---|
| **ZJUT-2a** | **2.6** | **10** | **This work** |
| MAF-23-O | 1.3 | 15 | 11 |
| KAUST-7[c] | 1.16 | 12 | 10 |
| Co-MOF-74[c] | 6.50 | 6.48 | 4 |
| Y-abtc[c] | 1.26 | 8.3 | 8 |
| JNU-3a | 2.45 | 2.9 | 13 |
| Ni-NP | 2.30 | 9.6 | 16 |
| SIFSIX-3-Ni | 1.25 | 1.8 | 17 |
| TIFSIX-3-Ni | 0.8 | 2.0 | 17 |
| ZU-36-Co | 0.86 | 2.5 | 17 |
| ZU-36-Ni | 1.35 | 19 | 17 |
| SIFSIX-2-Cu-i | 2.00 | – | 5 |
| GeFSIX-2-Cu-i | 2.20 | – | 5 |

[a] Dynamic $C_3H_6$ uptake was obtained from breakthrough experiments.

[b] Dynamic $C_3H_6/C_3H_8$ selectivity was calculated from breakthrough curve.

[c] Dynamic uptake and selectivity were reported in ref. 16.

# Supplementary Figures

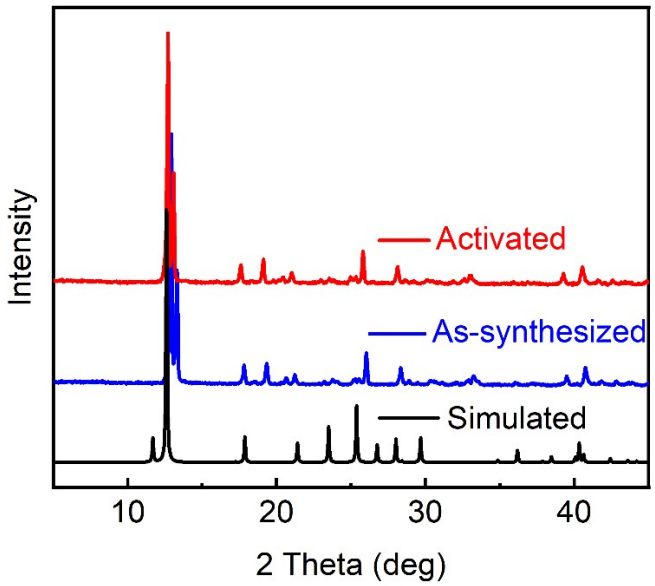


**Figure S1.** PXRD patterns of as-synthesized ZJUT-2 (red) and activated ZJUT-2a (blue) compared with the simulated PXRD pattern from the crystal structure of ZJUT-2 (black), which are consistent well with the PXRD patterns reported in our previous work.[1]

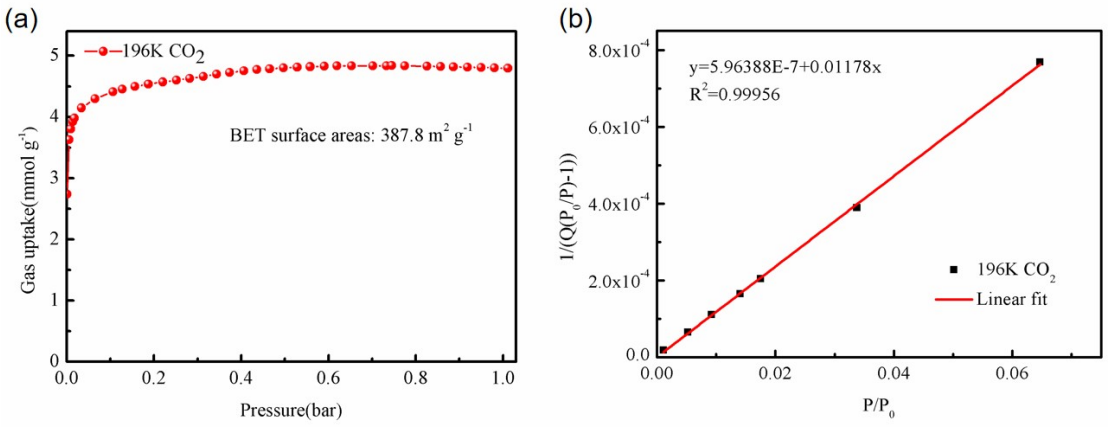


**Figure S2.** (a) 196 K $CO_2$ adsorption isotherms of ZJUT-2a. (b) BET calculation based on $CO_2$ adsorption isotherm of ZJUT-2a at 196 K.

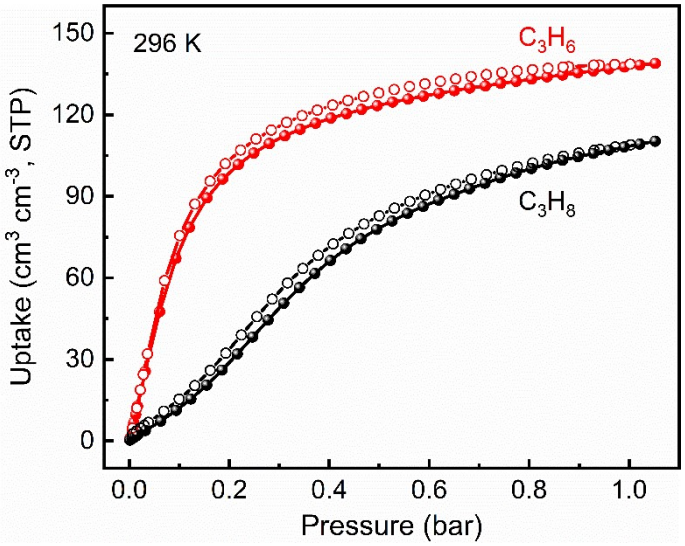


**Figure S3.** Adsorption isotherms of $C_3H_6$ (red) and $C_3H_8$ (black) for ZJUT-2a at 296 K up to 1 bar. Filled/empty circles represent adsorption/desorption.

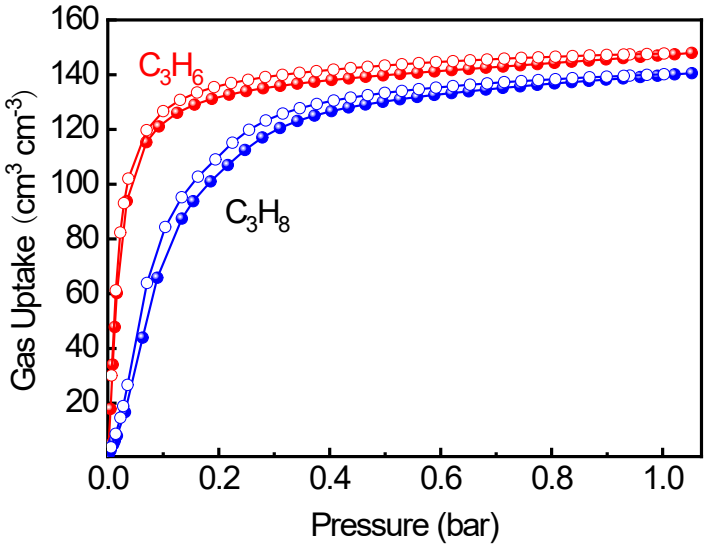


**Figure S4.** Adsorption isotherms of $C_3H_6$ (red) and $C_3H_8$ (blue) for ZJUT-2a at 273 K up to 1 bar. Filled/empty circles represent adsorption/desorption.

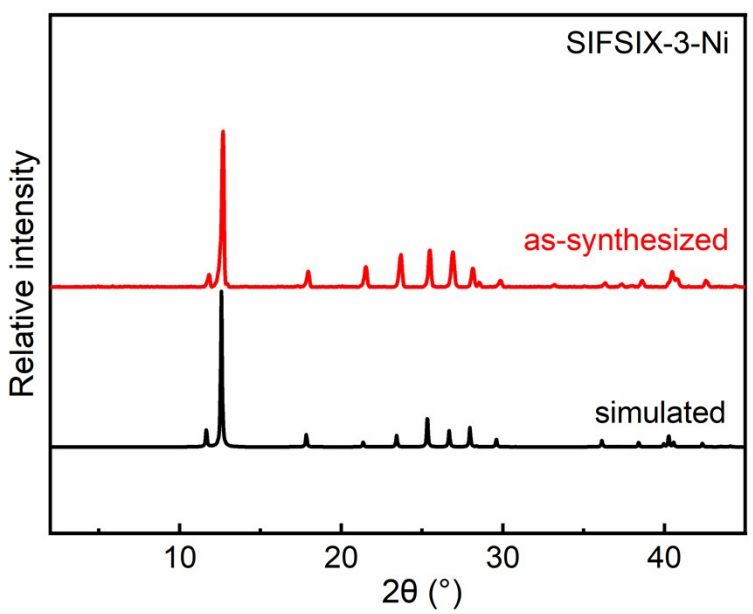


**Figure S5.** PXRD patterns of as-synthesized SIFSIX-3-Ni (red) compared with the simulated PXRD pattern from the crystal structure of SIFSIX-3-Ni (black).

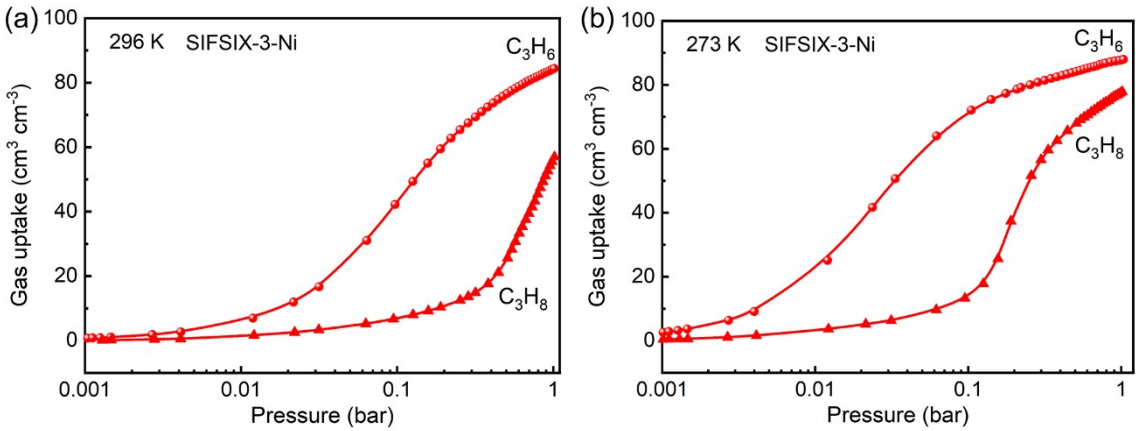


**Figure S6.** Adsorption isotherms of $C_3H_6$ (ball) and $C_3H_8$ (triangle) for SIFSIX-3-Ni at (a) 296 K and (b) 273 K up to 1 bar.

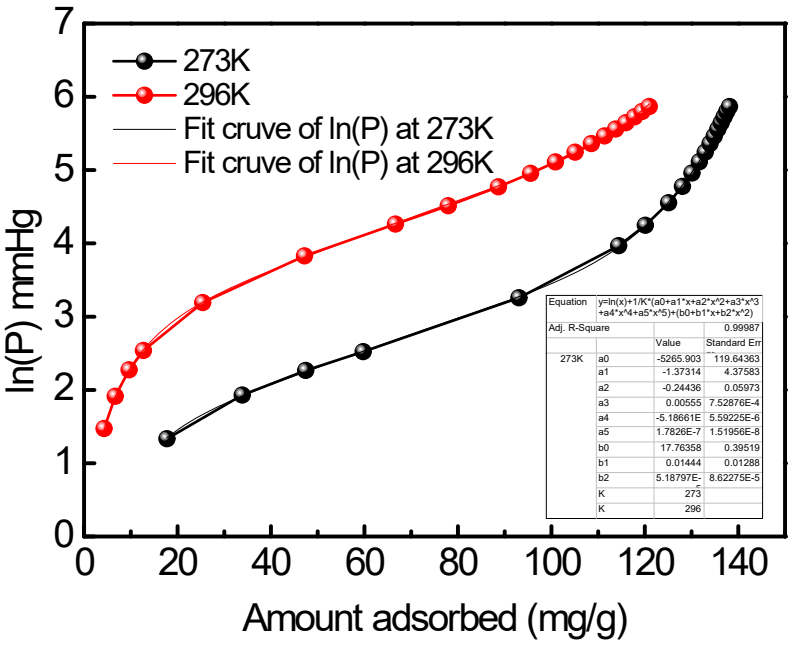


| Equation | y=ln(x)+1/K*(a0+a1*x+a2*x^2+a3*x^3+a4*x^4+a5*x^5)+(b0+b1*x+b2*x^2) | | |
|---|---|---|---|
| Adj. R-Square | | | 0.99987 |
| | | Value | Standard Err |
| 273K | a0 | -5265.903 | 119.64363 |
| | a1 | -1.37314 | 4.37583 |
| | a2 | -0.24436 | 0.05973 |
| | a3 | 0.00555 | 7.52876E-4 |
| | a4 | -5.18661E | 5.59225E-6 |
| | a5 | 1.7826E-7 | 1.51956E-8 |
| | b0 | 17.76358 | 0.39519 |
| | b1 | 0.01444 | 0.01288 |
| | b2 | 5.18797E-5 | 8.62275E-5 |
| | K | 273 | |
| | K | 296 | |

**Figure S7.** Virial fitting of the $C_3H_6$ adsorption isotherms for ZJUT-2a.

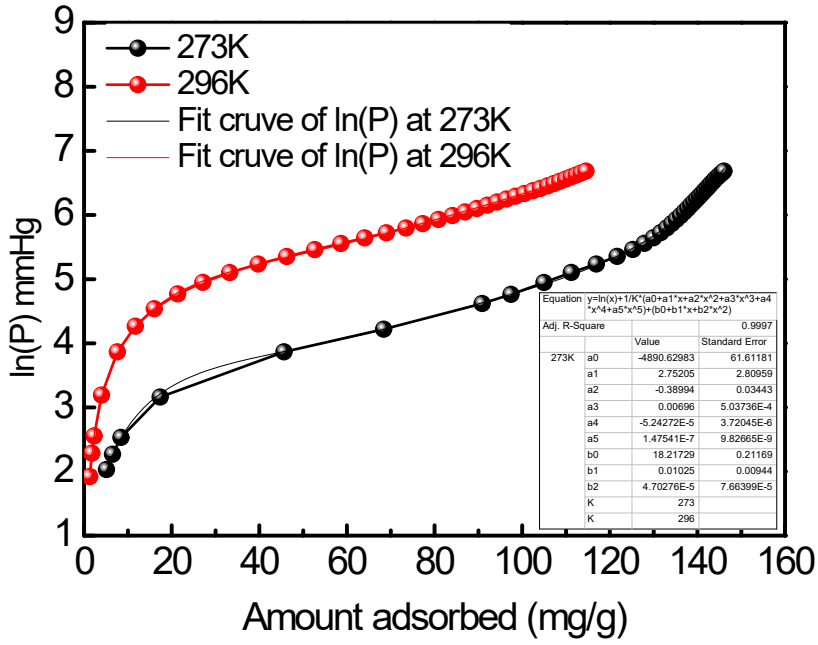


| Equation | y=ln(x)+1/K*(a0+a1*x+a2*x^2+a3*x^3+a4*x^4+a5*x^5)+(b0+b1*x+b2*x^2) | | |
|---|---|---|---|
| Adj. R-Square | | | 0.9997 |
| | | Value | Standard Error |
| 273K | a0 | -4890.62983 | 61.61181 |
| | a1 | 2.75205 | 2.80959 |
| | a2 | -0.38994 | 0.03443 |
| | a3 | 0.00696 | 5.03736E-4 |
| | a4 | -5.24272E-5 | 3.72045E-6 |
| | a5 | 1.47541E-7 | 9.82665E-9 |
| | b0 | 18.21729 | 0.21169 |
| | b1 | 0.01025 | 0.00944 |
| | b2 | 4.70276E-5 | 7.66399E-5 |
| | K | 273 | |
| | K | 296 | |

**Figure S8.** Virial fitting of the $C_3H_8$ adsorption isotherms for ZJUT-2a.

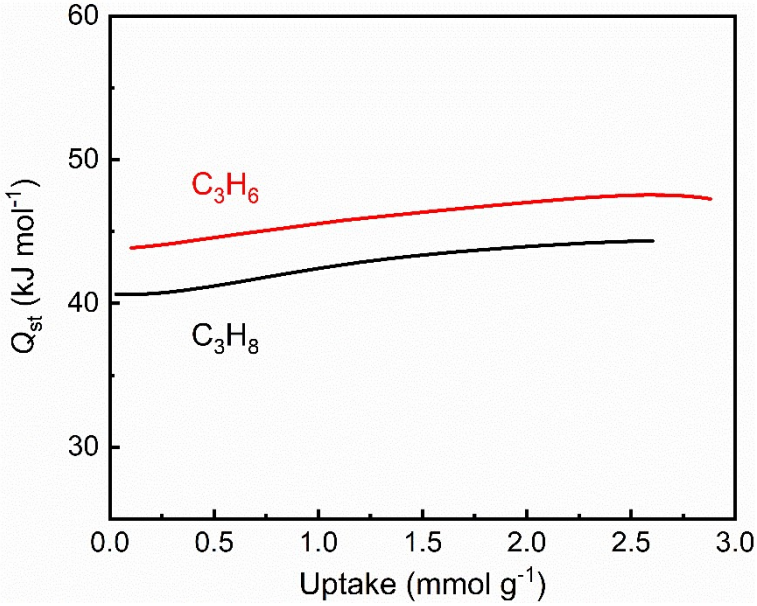


**Figure S9.** Heats of adsorption ($Q_{st}$) of $C_3H_6$ (red) and $C_3H_8$ (black) for ZJUT-2a.

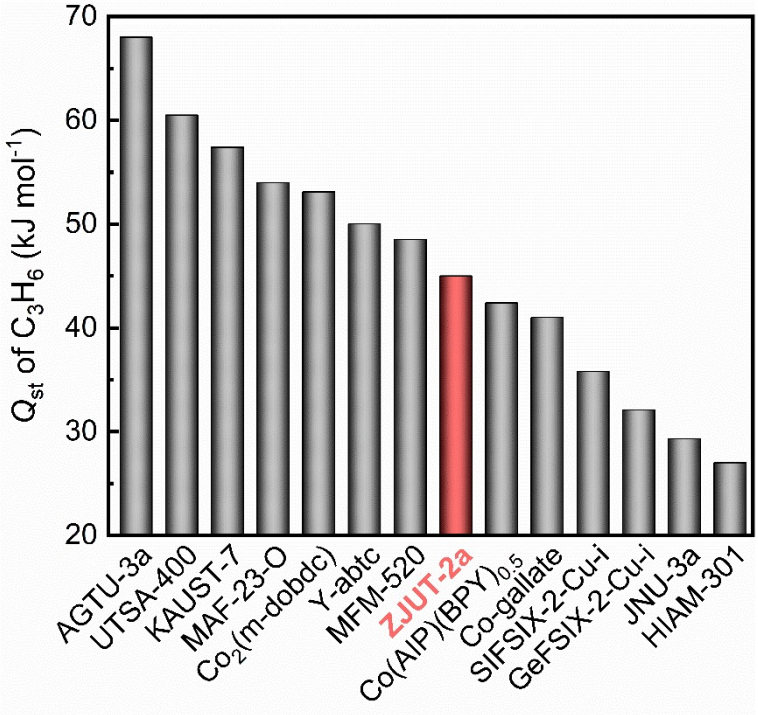


**Figure S10.** Comparison of heats of adsorption ($Q_{st}$) of $C_3H_6$ for ZJUT-2a and other reported materials.

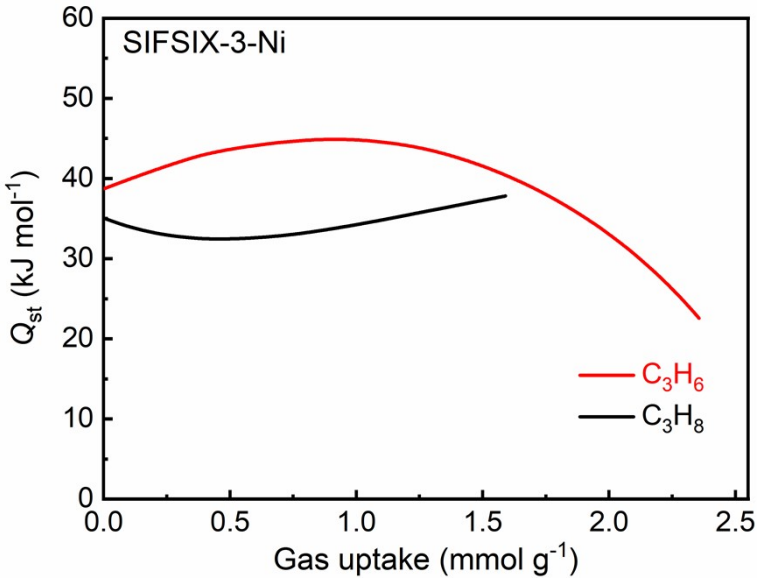


**Figure S11.** Heats of adsorption ($Q_{st}$) of $C_3H_6$ (red) and $C_3H_8$ (black) for SIFSIX-3-Ni.

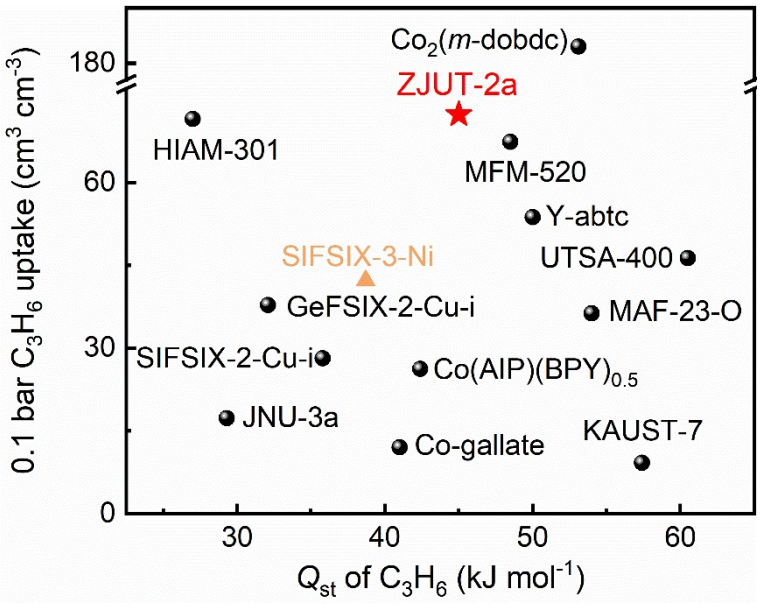


**Figure S12.** Comparison of heats of adsorption ($Q_{st}$) of $C_3H_6$ and 0.1 bar $C_3H_6$ uptake for ZJUT-2a and other reported materials.

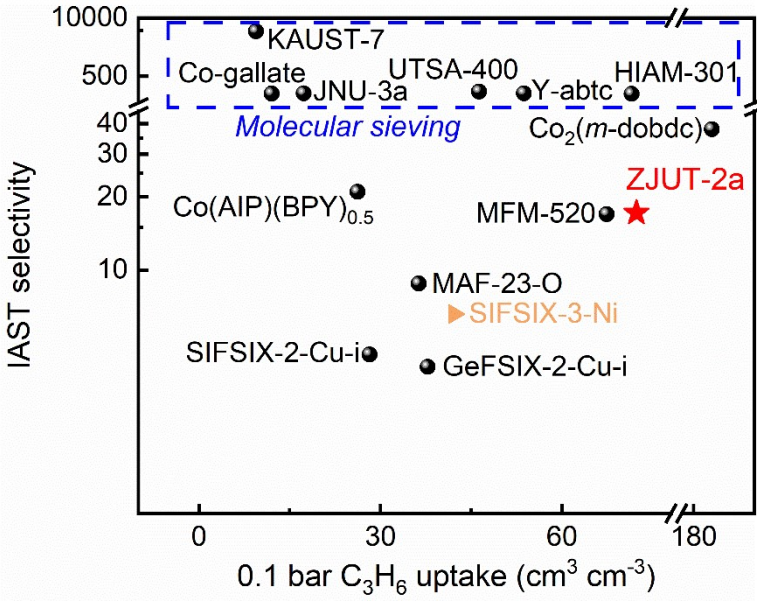


**Figure S13.** Comparison of $C_3H_6/C_3H_8$ IAST selectivity and 0.1 bar $C_3H_6$ uptake for ZJUT-2a and other reported materials.

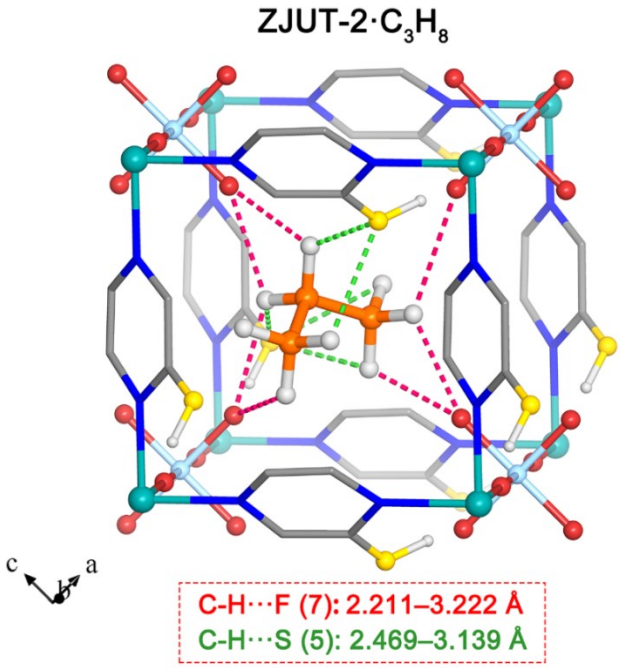


**Figure S14.** Illustration of $C_3H_8$ adsorption site in the nano-trap of ZJUT-2a, revealed by theoretical calculations.

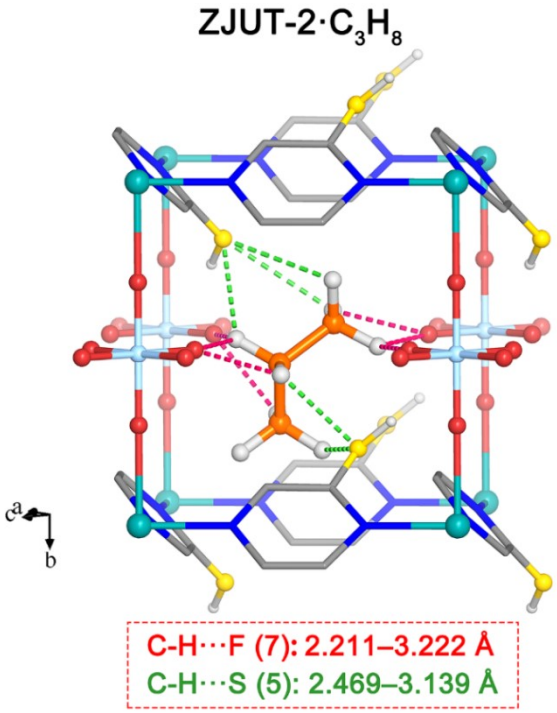


**Figure S15.** Illustration of $C_3H_8$ adsorption site in the nano-trap of ZJUT-2a, revealed by theoretical calculations.

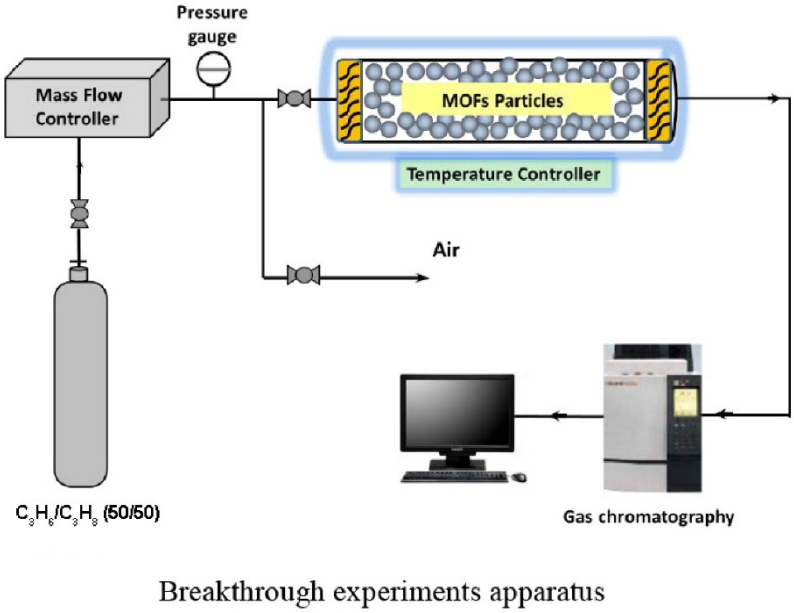


**Figure S16.** Schematic illustration of the apparatus for the breakthrough experiments.

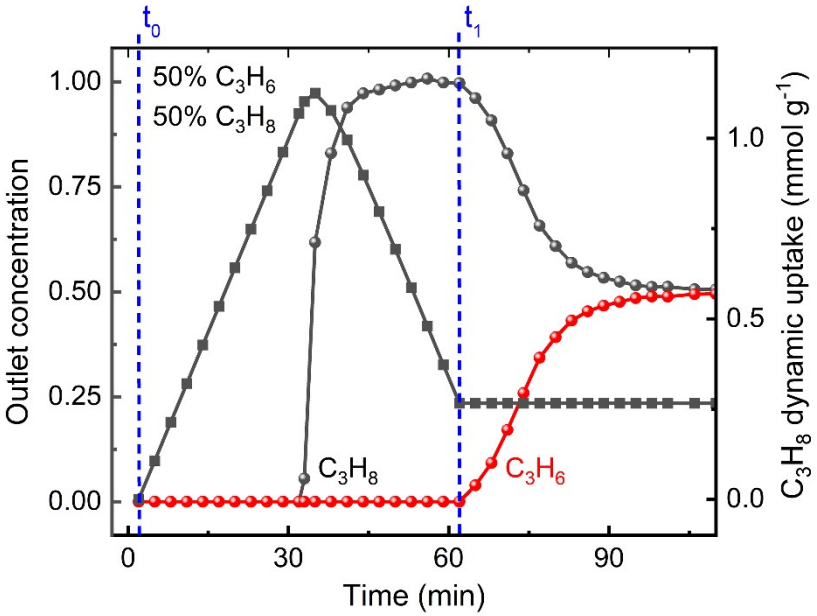


**Figure S17.** Experimental column breakthrough curves (circle) and $C_3H_8$ dynamic uptake calculation (square) for a 50/50 $C_3H_6$/$C_3H_8$ mixture in ZJUT-2a. The calculation of dynamic uptake is based on equation (6). Dashed blue lines: $C_3H_8$ gas adsorbed from $t_0$ to $t_1$ (62 min) when the $C_3H_6$ breakthrough occurred.

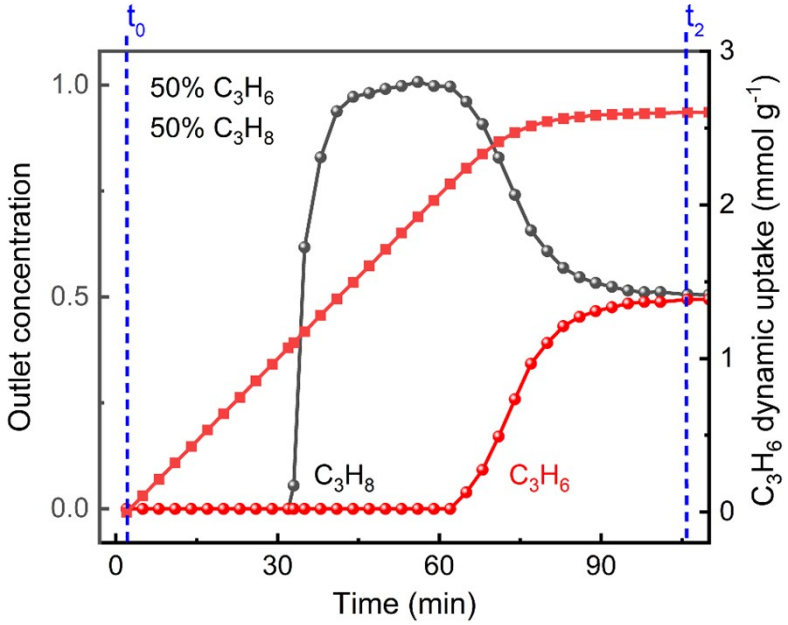


**Figure S18.** Experimental column breakthrough curves (circle) and $C_3H_6$ dynamic uptake calculation (square) for a 50/50 $C_3H_6$/$C_3H_8$ mixture in ZJUT-2a. The calculation of dynamic uptake is based on equation (6) and the dynamic selectivity is calculated based on equation (7). Dashed blue lines: $C_3H_6$ gas adsorbed from $t_0$ to $t_2$ (106 min) when the $C_3H_6$ breakthrough was completed.

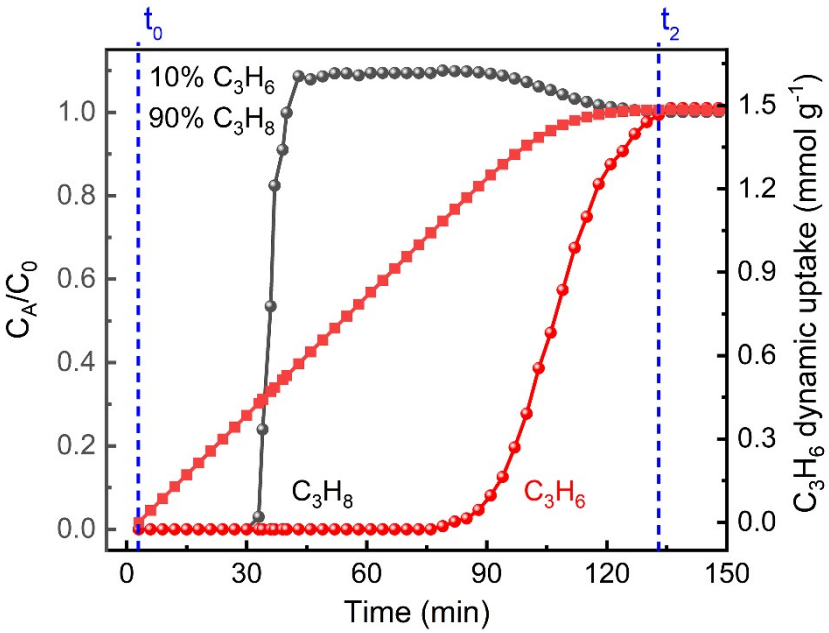


**Figure S19.** Experimental column breakthrough curves (circle) and $C_3H_6$ dynamic uptake calculation (square) for a 10/90 $C_3H_6/C_3H_8$ mixture in ZJUT-2a. The calculation of dynamic uptake is based on equation (6). Dashed blue lines: $C_3H_6$ gas adsorbed from $t_0$ to $t_2$ (133 min) when the $C_3H_6$ breakthrough was completed.

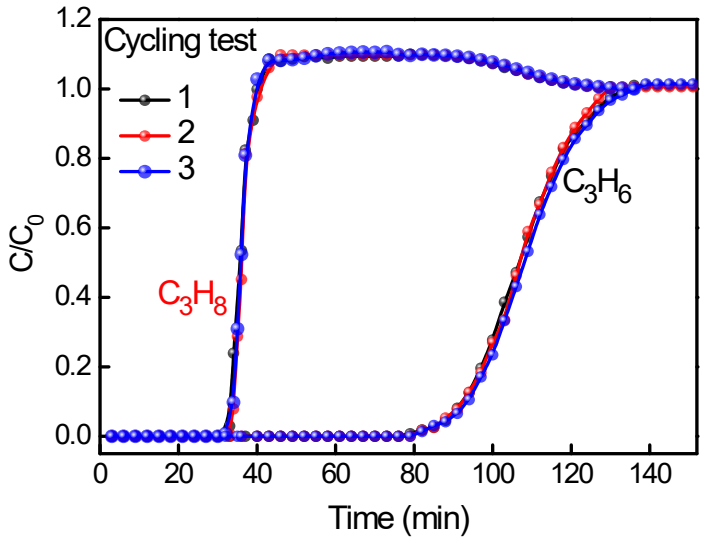


**Figure S20.** Cycling column breakthrough curves for $C_3H_6/C_3H_8$ separation (10/90, v/v) with ZJUT-2a at 296 K and 1.0 bar.

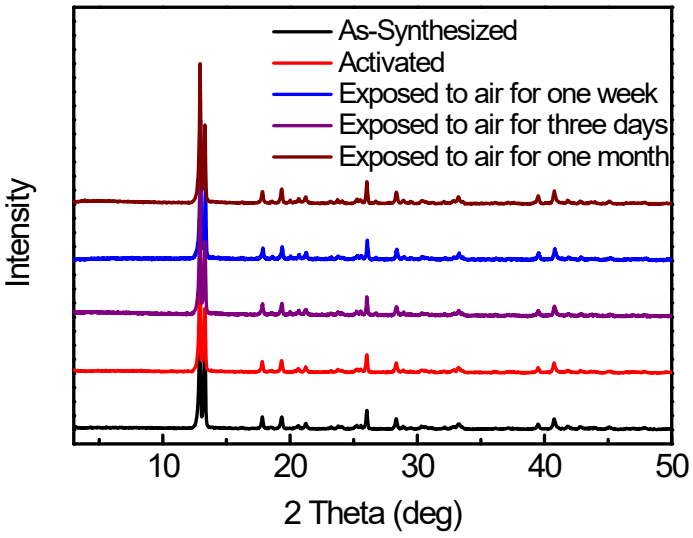


**Figure S21.** PXRD patterns of as-synthesized ZJUT-2 (black), activated ZJUT-2a (red), and ZJUT-2 samples exposed to air for three days (purple), one week (blue) and one month (wine), indicating its great air stability.

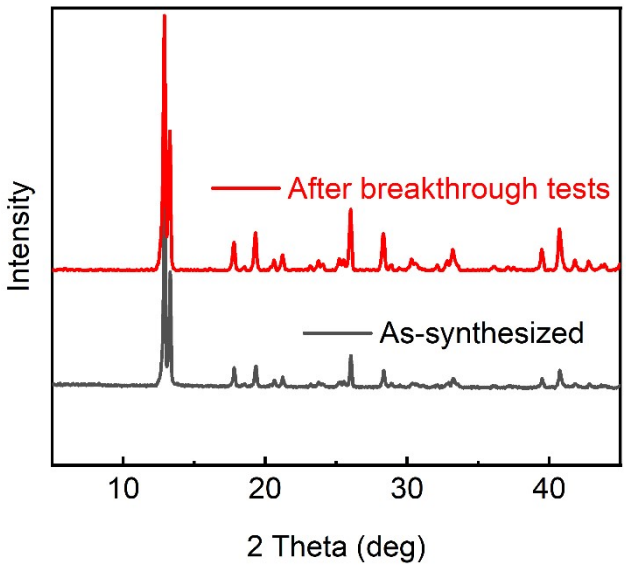


**Figure S22.** PXRD patterns of as-synthesized ZJUT-2 (black) and ZJUT-2 samples after multiple breakthrough tests (red).

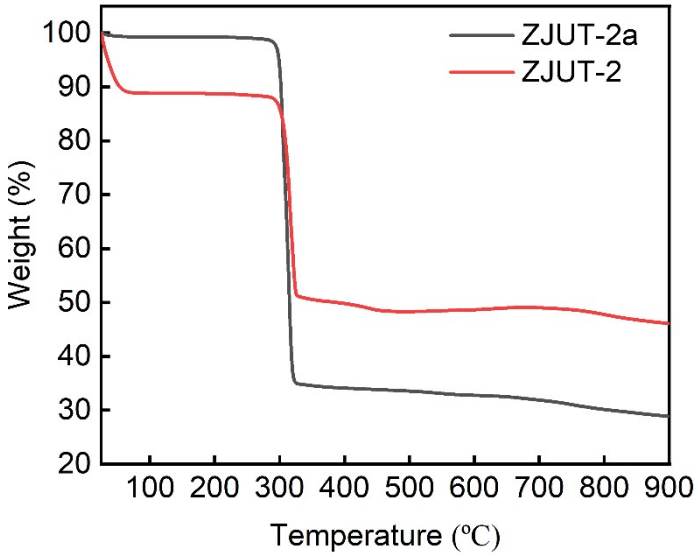


**Figure S23.** TGA curves of synthesized (black) and activated (red) ZJUT-2 samples under a flow of $N_2$ at a rate of 5 °C $min^{-1}$.

# Supplementary References


[1] H.-M. Wen, C. Liao, L. Li, L. Yang, J. Wang, L. Huang, B. Li, B. Chen and J. Hu, *Chem. Commun.*, 2019, **55**, 11354–11357.

[2] A. L. Myers, J. M. Prausnitz, *AIChE J.*, 1965, **11**, 121−127.

[3] J. E. Bachman, M. T. Kapelewski, D. A. Reed, M. I. Gonzalez and J. R. Long, *J. Am. Chem. Soc.*, 2017, **139**, 15363–15370.

[4] Y.-S. Bae, C. Y. Lee, K. C. Kim, O. K. Farha, P. Nickias, J. T. Hupp, S. T. Nguyen and R. Q. Snurr, *Angew. Chem. Int. Ed.*, 2012, **51**, 1857–1860.

[5] X. Wang, P. Zhang, Z. Zhang, L. Yang, Q. Ding, X. Cui, J. Wang and H. Xing, *Ind. Eng. Chem. Res.*, 2020, **59**, 3531–3537.

[6] B. Liang, X. Zhang, Y. Xie, R.-B. Lin, R. Krishna, H. Cui, Z. Li, Y. Shi, H. Wu, W. Zhou and B. Chen, *J. Am. Chem. Soc.*, 2020, **142**, 17795–17801.

[7] L. Yu, X. Han, H. Wang, S. Ullah, Q. Xia, W. Li, J. Li, I. da Silva, P. Manuel, S. Rudić, Y. Cheng, S. Yang, T. Thonhauser and J. Li, *J. Am. Chem. Soc.*, 2021, **143**, 19300–19305.

[8] H. Wang, X. Dong, V. Colombo, Q. Wang, Y. Liu, W. Liu, X.-L. Wang, X.-Y. Huang, D. M. Proserpio, A. Sironi, Y. Han and J. Li, *Adv. Mater.*, 2018, **30**, 1805088.

[9] H. Wu, Y. Yuan, Y. Chen, F. Xu, D. Lv, Y. Wu, Z. Li and Q. Xia, *AIChE J.*, 2020, **66**, e16858.

[10] A. Cadiau, K. Adil, P. M. Bhatt, Y. Belmabkhout and M. Eddaoudi, *Science*, 2016, **353**, 137–140.

[11] Y. Wang, N.-Y. Huang, X.-W. Zhang, H. He, R.-K. Huang, Z.-M. Ye, Y. Li, D.-D. Zhou, P.-Q. Liao, X.-M. Chen and J.-P. Zhang, *Angew. Chem. Int. Ed.*, 2019, **58**, 7692–7696.

[12] Y. Xie, Y. Shi, E. M. C. Morales, A. E. Karch, B. Wang, H. Arman, K. Tan and B. Chen, *J. Am. Chem. Soc.*, 2023, **145**, 2386–2394.

[13] H. Zeng, M. Xie, T. Wang, R.-J. Wei, X.-J. Xie, Y. Zhao, W. Lu and D. Li, *Nature*, 2021, **595**, 542–548.

[14] J. Li, X. Han, X. Kang, Y. Chen, S. Xu, G. L. Smith, E. Tillotson, Y. Cheng, L. J. McCormick Mcpherson, S. J. Teat, S. Rudić, A. J. Ramirez-Cuesta, S. J. Haigh, M. Schröder and S. Yang, *Angew. Chem. Int. Ed.*, 2021, **60**, 15541–15547.

[15] D. Liu, J. Pei, X. Zhang, X.-W. Gu, H.-M. Wen, B. Chen, G. Qian and B. Li, *Angew. Chem. Int. Ed.*, 2023, **62**, e202218590.

[16] Y. Xie, Y. Shi, H. Cui, R.-B. Lin and B. Chen, *Small Struct.*, 2022, **3**, 2100125.

[17] Z. Zhang, Q. Ding, X. Cui, X.-M. Jiang and H. Xing, *ACS Appl. Mater. Interfaces*, 2020, **12**, 40229–40235.